Analyst

Microfluidic-Electrochemical Sensor utilizing Statistical Modeling for Enhanced Nitrate Detection in Surface Water towards Environmental Monitoring

Journal:	*Analyst*
Manuscript ID	AN-ART-01-2025-000092.R1
Article Type:	Paper
Date Submitted by the Author:	25-Mar-2025

Complete List of Authors:	Mani, Sai; University of Maryland Baltimore County Kadolkar, Revati; University of Maryland Baltimore County Prajapati, Tithi; University of Maryland Baltimore County Ahuja, Preety; University of Maryland Baltimore County Shajahan, Mesha ; University of Maryland Baltimore County Lee, JungHun; University of Maryland Baltimore County Tolosa, Michael; University of Maryland Baltimore County McWilliams, Mary; University of Maryland Baltimore County Welty, Claire; University of Maryland Baltimore County Frey, Douglas ; University of Maryland Baltimore County Srinivasan, Venkatesh; University of Maryland Baltimore County Ujjain, Sanjeev; University of Maryland Baltimore County Rao, Govind; University of Maryland Baltimore County, Center for Advanced Sensor Technology (CAST)

ARTICLE

Microfluidic-Electrochemical Sensor utilizing Statistical Modeling for Enhanced Nitrate Detection in Surface Water towards Environmental Monitoring

Received 00th January 20xx,
Accepted 00th January 20xx

DOI: 10.1039/x0xx00000x

Sai Kiran Mani†[a], Revati Kadolkar†[a,b], Tithi Prajapati[a,d], Preety Ahuja[a], Mesha Shajahan[a,d], JungHun Lee[a,b], Michael Tolosa[a], Mary McWilliams[c], Claire Welty[b,c], Douglas D. Frey[a,b], Venkatesh Srinivasan[a], Sanjeev Kumar Ujjain*[a] and Govind Rao*[a,b]

Nitrate (NO_3^-) presence in surface water and groundwater used for potable supply needs to be closely monitored since elevated amounts can adversely affect the aquatic life and human health by causing hypoxia and methemoglobinemia. Many of the existing EPA-certified sensors used for environmental monitoring are expensive, bulky, and labor-intensive. To address these concerns, we have successfully developed a low-cost microfluidic electrochemical impedimetric sensor, consisting of a nitrate-binding nickel complex within a polyaniline/carbon nanocomposite (Ni@Pani/C) enabling nitrate monitoring in field. Under optimized conditions, our sensor demonstrated a high sensitivity of 2.31±0.09 Ω/ppm/cm^2 across a wide nitrate concentration range (0.6-10 ppm). It also showed a desirable low detection limit of 0.015 ppm and a swift response time under 20 seconds. It maintained repeatability over a wide temperature range (5-65°C) and exhibited consistent performance over an extended period (~1 month). The sensor displayed high specificity towards nitrate when tested against potential interferences (SO_4^{2-}, $C_2H_3O_2^-$, HCO_3^-, NH_4^+, Cl^-) and showed good reproducibility for test water samples collected from various streams in Maryland, U.S.A. A statistical model was used to confirm the sensor's accuracy, which yielded a maximum standard deviation of ±0.6 ppm (absolute value). Our sensor was also benchmarked against a commercial SUNA device resulting in comparable performance.

Introduction

The availability of high-quality drinking water is the 6th out of 17 Sustainable Development Goal (SDG) global indicators listed by the United Nations.[1] Continuous monitoring of water quality is increasingly becoming a necessity due to the constant release of toxic effluents to surface water and groundwater. Nitrate (NO_3^-) is one such contaminant that is released into the environment through synthetic and agricultural fertilizers, livestock manure discharge, atmospheric deposition, septic system discharge, and sanitary sewer leaks.[2] Nitrate contamination is a global concern owing to reliance on surface water and groundwater sources for potable water supply. High nitrate contamination can lead to algal blooms in lakes, rivers and estuaries, resulting in oxygen-depleted zones causing hypoxia in aquatic life.[3] In humans, nitrate can lead to gastric cancer as nitrites form carcinogenic N-nitrosamines upon interaction with amines/amides in the stomach[3-8]. Prolonged nitrate exposure may result in birth defects, spontaneous abortion, intrauterine growth restriction, and methemoglobinemia, also called the blue baby syndrome, which results from binding of nitrate to haemoglobin, thereby causing depletion of oxygen in body tissues[9,10]. To address these concerns, the World Health Organization (WHO) has established a maximum allowable concentration of 10 mg/L or 10 ppm of nitrate-nitrogen (equivalent to 50 mg/L of nitrate ion) in drinking water.[11] However, there is a lack of low-cost and sensitive real-time commercial sensors for the continuous monitoring of nitrate contamination through frequent testing[12-14].

One of the reasons for unavailability of such sensors is the inherent complexities in direct and indirect measurement techniques of nitrate, namely electrophoresis and polarography.[15] Typically, nitrate (NO_3^-) is first reduced to nitrite ions (NO_2^-) and then quantified using spectrophotometry. This approach has multiple steps, large interferences and a limited detection range.[17] Various alternative laboratory techniques used for nitrate detection, such as colorimetry[18,19], molecular imprinting[20], ion chromatography[21,22] and field-effect transistor technology[23] involve labor-intensive sampling, require advanced instrumentation, and are time-consuming.[13] Commercially available sensors that are highly selective for nitrate typically need frequent calibration.[24]

[a] Center for Advanced Sensor Technology, Department of Chemical, Biochemical and Environmental Engineering, University of Maryland Baltimore County, Baltimore, MD 21250, USA.
[b] Department of Chemical, Biochemical and Environmental Engineering, University of Maryland Baltimore County, Baltimore, MD 21250, USA.
[c] Center for Urban Environmental Research and Education, University of Maryland Baltimore County, Baltimore, MD 21250, USA.
[d] Department of Biological Sciences, University of Maryland Baltimore County, Baltimore, MD, 21250, USA.
† S. K. Mani, and R. Kadolkar contributed equally to this work.
Supplementary Information available: [details of any supplementary information available should be included here]. See DOI: 10.1039/x0xx00000x

In contrast to these sensing methodologies, potentiometric and electrochemical techniques are simple, rapid, cost-effective and offer a direct quantitative analysis of targeted ions in field samples[13,14]. Nanomaterial-based electrochemical sensors have emerged as powerful analytical tools, characterized by their reduced over-potential and high sensitivity. Usage of transition metals like copper, silver, palladium, cobalt, nickel, rhodium, gold and platinum, has further demonstrated electroreduction capabilities for nitrate.[25] However, nitrate can contaminate the surfaces of these metallic substrates leading to unsatisfactory sensing performance.[26] Electrochemical nitrate sensing that relies on oxidation reactions of such materials and primarily composed of copper or silver, usually encounters interference from other oxidizable species.[13] One effective approach to enhance the selectivity of metallic nanoparticles towards nitrate involves the use of modified functional materials aimed at minimizing operational electrode potential.[27] Among such functional materials, conducting polymers like polyaniline (Pani) have shown promise for electrochemical sensing due to their bio compatibility, low toxicity, facile synthesis, cost-effective large-scale production, electro-active redox potentials, high capacity to stabilize enzymes, and the ability to anchor metal nanoparticles with the aid of amino groups[9,28].

Pani can store electrical energy during redox transition, namely the transition between fully reduced leucoemeraldine base (LB) ↔ semi-oxidized emeraldine salt (ES) and ES ↔ fully oxidized pernigraniline base (PB), depending on the sensing mechanism (i.e., oxidation or reduction)[29,30]. Pani has shown the ability to adsorb and electrocatalytically reduce nitrate within a low potential range, without causing electrode fouling.[31] Indirect measurement of nitrate is thus possible based on the electrochemical oxidation current generated during the ES↔PB redox transition of Pani.[32]

Pani-carbon composites, in this context, are frequently preferred due to carbon's (graphene or CNT) versatility as an electrode modifier and the ability to facilitate an enhanced electron transfer between the electroactive analytes and electrode surfaces.[32] A carbon matrix helps to improve the electrical conductivity of Pani by creating a porous structure with highly accessible surface area that enhances mass transport of the target analyte resulting in a direct redox reaction.[33] Pani/CNT electrodes have been recently explored for the electrochemical detection of nitrate in tap water, where the oxygen functional groups in CNT adsorb radical cations in the ES form of Pani, thereby making it thermodynamically more favourable for nitrate complex formation.[34] However, the sensing performance of Pani still depends on the synthesis method, morphology, and loading amount.[35] While graphene and CNT-based nanocomposites offer high electrical conductivity, their practical applications in electrochemical sensors can be hindered by issues such as production scalability and functionalization complexities. Amorphous carbon-based nanocomposites, on the other hand, overcome these concerns making them more suitable for sensor applications despite having lower conductivity and mechanical strength[36-38]. Such carbon materials with established safety profiles can streamline regulatory approvals and gain greater market acceptance. Given this background, we have chosen to integrate these concepts by utilizing a Pani-carbon (Pani/C) composite with the well-established nickel (Ni^{2+}) and nitriloacetic acid (NTA) complexation system[39,40]. Ni^{2+} has been proven to be a multifunctional and low-cost nanoparticle for nitrate binding[41], while NTA-functionalized polymers can be easily adsorbed on amorphous carbon. NTA is a tetradentate ligand that forms a hexagonal complex with a divalent metal ion (here Ni^{2+}) without affecting the electrochemical performance of Pani.[42]

Additionally, the Ni^{2+}/Pani composite has been proven to be thermodynamically stable for the electrochemical sensing of nitrite, with anti-interference ability in the presence of several metal ions.[43] Doping of NTA in the upper layers of Pani has also shown enhanced electrochemical properties by increasing the anodic peak potential (or oxidation peak current).[42] However, the use of Ni-NTA incorporated Pani/C for the detection of nitrate in water has not been reported yet, and this study aims to explore that application. Based on Pani's demonstrated ability for nitrate reduction and indirect detection at low potentials without electrode fouling, as well as the multifunctional role of Ni^{2+} in nitrate binding and NTA's metal complexation ability for easy adsorption on carbon materials, we have developed a Ni-NTA embedded Pani/C nanocomposite in this study (Ni@Pani/C).

This paper presents the development of an electrochemical impedimetric sensor integrated into a cost-effective polymethyl methacrylate (PMMA) microfluidic cassette (Figure 1). The objective of this work is to develop a miniaturized, low-cost, low-carbon footprint and field-deployable nitrate sensor. The microfluidic sensor developed in this study was tested for its measurement equivalency with a commercial SUNA V2 nitrate sensor while assessing water samples collected from various streams in Maryland, U.S.A. Additionally, the accuracy of our sensor's measurements was investigated with a statistical model developed in MATLAB that explores regression analysis and provides a three-dimensional (3D) calibration plot. Based on the charge transfer resistance (R_{CT}) obtained from experimental electrochemical data, the model can directly predict nitrate concentrations (ppm) in corresponding field water samples. Overall, in this paper it can be observed that our sensor offers several advantages such as a vast detection range, high sensitivity, fast response rate, temperature durability, long-term consistency, reliability against potential interferences, precision, simple analysis supported by a computational model, scalable fabrication, affordability, and environmental sustainability as opposed to the commonly observed challenges with portable sensors[12-14,24-26]

Results and Discussion

Morphology and Functionality

Figure 1A-F illustrates a schematic representation of Ni@Pani/C, coated graphite electrode, microfluidic cassette and nitrate sensing data. Surface morphology of the Ni@Pani/C nanocomposite investigated by SEM showed pseudo-spherical and interconnected granular nanoparticles (Figures 1B and

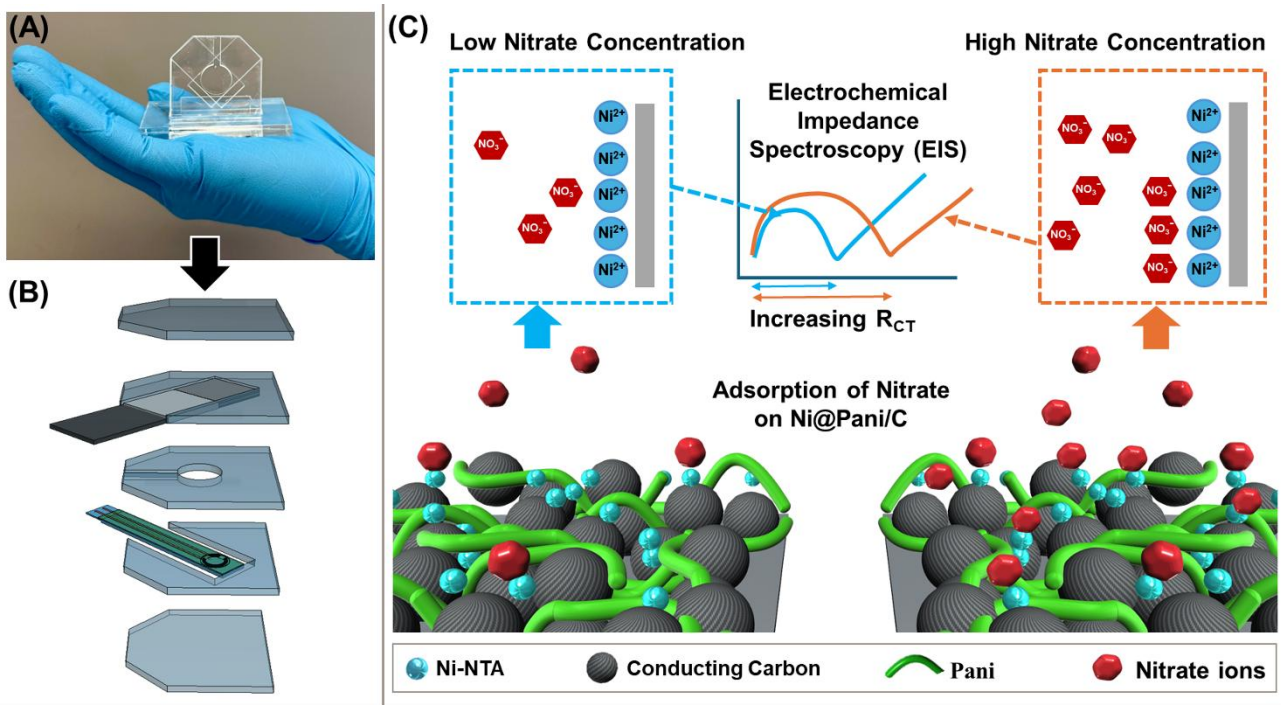

Fig. 1 Schematic showing (A) the custom fabricated microfluidic cassette; (B) an expanded view of the PMMA layers of the microfluidic cassette; (C) a 3D rendering of the nickel complex polyaniline carbon (Ni@Pani/C) nanocomposite showing adsorbed nitrate ions, and corresponding charge transfer resistance (R_{CT}) observed in electrochemical impedance spectroscopy (EIS).

S1A). Elemental mapping performed using EDX showed uniform and continuous distribution of carbon (C), oxygen (O) and nitrogen (N) with spatially distributed nickel (Ni) (Figure S1B). The TEM image demonstrated inter-woven circular structure of carbon with uniformly distributed, non-aggregated Pani nanoparticles on carbon (Pani/C) (Figure S1C). Pani seemed to be selectively deposited on the surface of carbon.

Optimization and Electrochemical Methods

Optimization of experimental conditions was performed in a three-electrode cell setup as presented in Figure S2.[44] A 3D schematic of this well-established setup used extensively for electrochemical sensing is shown in Figure 2A inset. This setup laid the groundwork for validating our sensing electrode's performance and for scaling down the device into a microfluidic chip, which shall eventually be used for field analysis. Impedance results from Nyquist plots observed in the magnified image in Figure 2A outset show a smaller semi-circle in the high frequency region, as well as a lower R_{CT} value (R_{CT} ≈ 8 Ω) compared to Pani/C (R_{CT} ≈ 44 Ω) and bare graphite electrode (R_{CT} ≈ 210 Ω).

These findings suggest that Ni@Pani/C may enhance the transport of the ferricyanide/ferrocyanide redox couple.[44] Ni@Pani/C has also shown a three times higher diffusion coefficient (D_a) of ions ($5.0x10^{-7}$ cm^2 sec^{-1}) compared to Pani/C ($1.7x10^{-7}$ cm^2 sec^{-1}) (Figure 2B). This indicates an enhanced diffusion and transport of electrolytic ions in both vertical and horizontal directions within the Ni@Pani/C film. A combination of low R_{CT}, high conductivity and increased D_a in Ni@Pani/C indicates the possibility of an enhanced electron transfer between the electrochemical probe and base graphite electrode. The impact of scan rate on electrochemical behavior of the Ni@Pani/C electrode can be observed in Figure S3A. With increasing scan rates, CV graphs show a slight shift in the positive direction for the anodic peak (E_a) and in negative direction for the cathodic peak (E_c). Broadening of distances between the anodic and cathodic peaks signifies a quasi-reversible transition between ES↔PB states of Pani.[34] Additionally, anodic (I_a) and cathodic (I_c) peak currents have also shown a linear and proportional increase with increasing scan rates (Figure S3B) at various pHs of the same electrolyte, thereby indicating a surface-controlled reversible process.[44] In the presence of nitrate, the ES↔PB redox transition has been proven to be controlled by both diffusion and adsorption mechanisms in the range of 30-50 mV/s scan rates.[33] Hence, a faster scan rate of 50 mV/s was chosen for all electrochemical CV sensing experiments in this study. CV graphs in Figure 2C display the three redox pairs of Pani corresponding to (i) LB↔ES transition, (ii) by-products and intermediates of the redox reaction, and (iii) ES↔PB transition of Pani.[29]

Moreover, two anodic peaks were observed at -0.18 V and -0.48 V, and the I_a at these peaks showed an increasing trend at higher pH (side image in Figure 2C). A shift in peak potentials and separation of the redox couples was also observed with increasing pH (Figure S4A), thereby indicating a high electrochemical reversibility of ES. Upon addition of 5 ppm nitrate to the same matrix, a reduction in the oxidation peak currents was observed (dotted traces in Figure 2C) for each of the three respective pHs. This decrease in current was comparable for both pH 6.0 and pH 7.0. Further, CV studies were performed with different electrolytes, since the protonation / deprotonation of Pani responsible for a complex

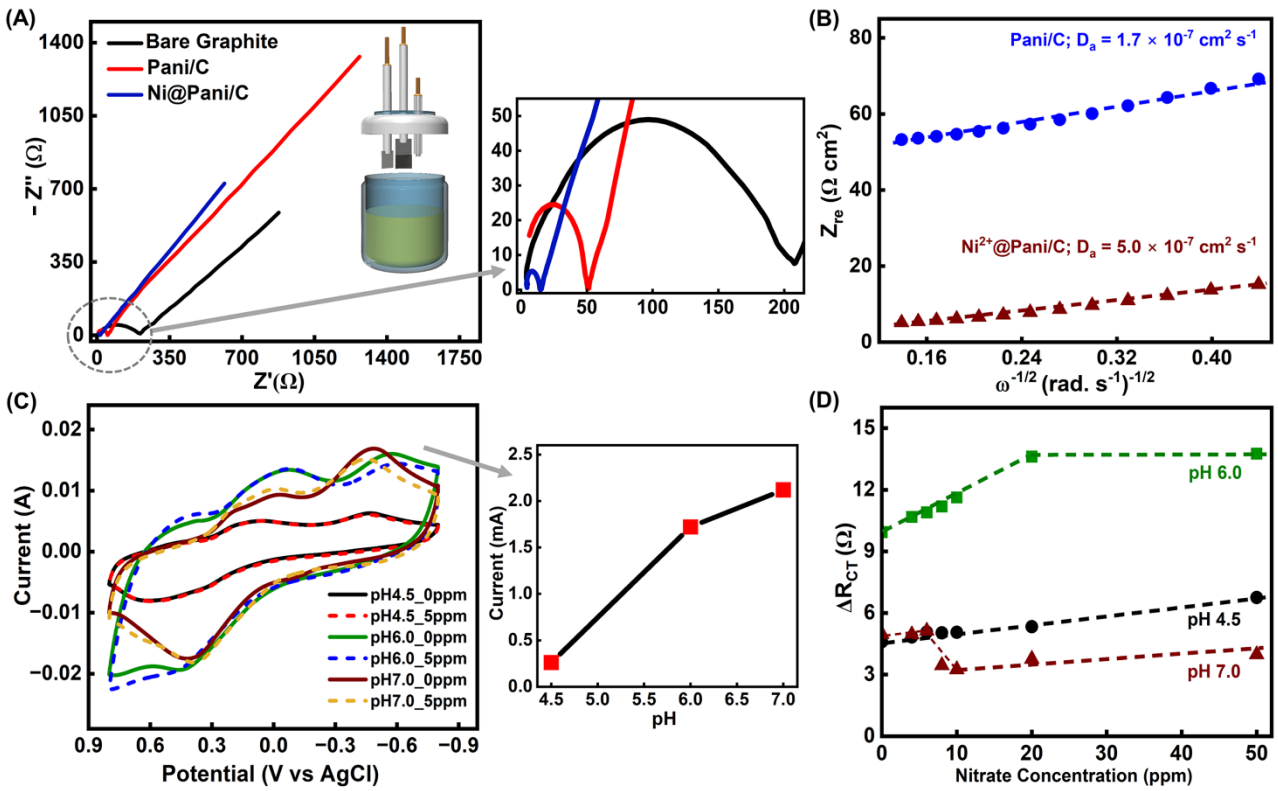

Fig. 2 (A) EIS Nyquist plot of bare graphite electrode (black), Pani/C (red) and Ni@Pani/C nanocomposite (blue) in 0.1 M PBS (pH 7.0) containing 5 mM [$K_3Fe(CN)_6$] and 0.1 M KCl. Outset: 3D schematic representation of the 75 mL conventional three electrode cell assembly; (B) Plot of |Z| vs. $\omega^{-1/2}$ from impedance data for Pani/C and Ni@Pani/C nanocomposite; (C) CV of Ni@Pani/C sensing electrode at 50 mV/s in the absence and presence of 5 ppm nitrate at electrolyte pH 4.5, 6.0 and 7.0, Outset: Plot showing change in current with pH; (D) Calibration curve of change in charge transfer resistance (ΔR_{CT}) in the Nyquist plot with increasing concentration of nitrate from 0-50 ppm for Ni@Pani/C sensor.

formation with nitrate is largely influenced by the electrolyte composition.[34] The 0.1 M KCl + 50 mM PBS + 100 mM $K_3Fe(CN)_6$ electrolyte demonstrated the most stable redox peaks (Figure S4B).

To understand the nitrate sensing behavior of this electrolyte, different pH conditions were tested[45] over a wide nitrate concentration ranging from 1-50 ppm using EIS (Figure 2D). The sensor was tested under different pH conditions to understand its behavior and performance. The sensor was sensitive to nitrate at all three pH conditions. However, a higher change in ΔR_{CT} was observed for pH 6.0, as compared to pH 4.5 and pH 7.0. At low pH, disruption of the coordination bond of the transition metal between NO_3^- and Ni^{2+} chelated by NTA can be responsible for inferior sensing behaviour.[46] It is also important to note that in highly acidic environments, nitrate reduces to other nitrogen containing species. While at neutral or slightly basic conditions, Pani transitions into its less conductive ES form and a sudden drop in ΔR_{CT} at pH 7.0 in Figure 2D can be attributed to various reasons. [20,32] A partial reprotonation of Pani could occur at higher nitrate concentrations at pH 7.0 from ion pairing, electrostatic screening or charge redistribution, thereby affecting the electrical double layer formation and resulting in a restoration of Pani's conductivity.[14,19,22,23] Overall, sensing at pH 6.0 showed consistent results and helped to avoid performance diminishing effects at slightly basic conditions. In the environment, since surface waters rarely have extreme acidic and basic pH conditions, our chosen pH 6.0 is ideal for field usage. Moreover, our field samples from the Patapsco region of the Piedmont physiographic province were expected to have a pH of 6.0-8.0.[47] Based on all of the above considerations, a buffer composition of 0.1 M KCl + 50 mM PBS + 100 mM $K_3Fe(CN)_6$ electrolyte with pH 6.0 was chosen for nitrate sensing in the CAST microfluidic (CAST-MF) electrochemical cassette.

Microfluidic Electrochemical Sensing

Miniaturization of the conventional 75 mL three-electrode electrochemical setup into a 500 µL microfluidic cassette significantly helped (i) to reduce the reagents used and waste generated, (ii) to lower the operational costs by minimizing resource consumption and waste disposal expenses, as well as (iii) to enhance sustainability by lowering the overall environmental footprint. In addition, the microfluidic system helps reduce the electrolyte volume to 500 µL and to enable a closer placement of the electrodes (0.5 mm). This provides high local ion density that leads to faster ionic interactions. Hence, the diffusion of ions from the bulk in a conventional macrosystem (75 mL) is slow and limited compared to that in a microfluidic system leading to sensitivity at higher nitrate concentrations in the latter. Figure 3A illustrates a 3D schematic and the corresponding experimental setup of the CAST-MF sensor. In addition to our fabricated working electrode (1cm^2), we utilized a pseudo-reference electrode and counter electrode from CAULYS to complete the three-electrode microfluidic

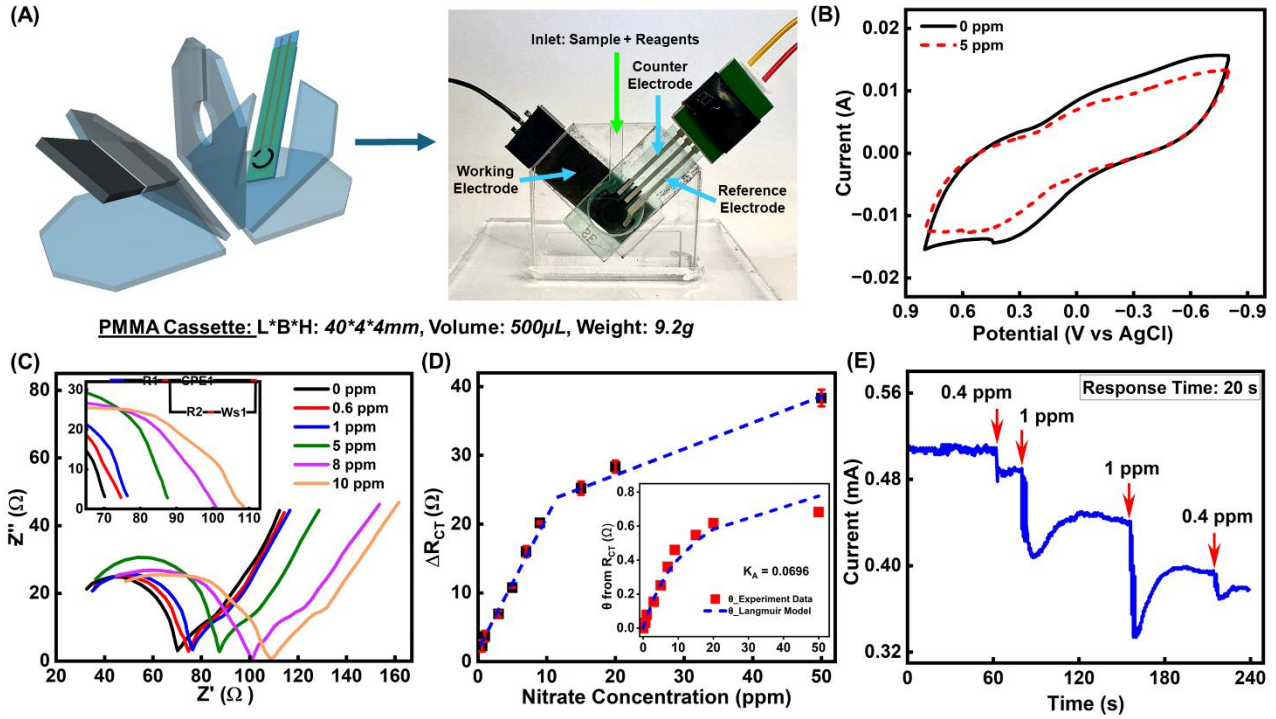

Fig. 3 (A) (Left) Schematic representation of the microfluidic cassette. (Right) PMMA-based microfluidic electrochemical sensor setup with Ni@Pani/C nanocomposite coated on 1 cm^2 graphite plate, screen-printed conducting carbon and Ag/AgCl working, counter and reference electrodes, respectively. Sample and reagents were pipetted through the top inlet slit. Description shows dimensions and weight of the microfluidic cassette; (B) CV plots of Ni@Pani/C CAST-MF sensor at 50 mV/s in the absence and presence of 5 ppm nitrate; (C) EIS Nyquist plots of Ni@Pani/C CAST-MF sensor upon successive injection of different concentrations of nitrate (0-10 ppm) in N_2 saturated 0.1 M PBS and pH 6.0 electrolyte at -0.45 V. Inset: Equivalent Randles circuit for fitting EIS results to analyze Nyquist plots, where solution resistance (R_S) is in series with a parallel combination of double-layer capacitance (CPE1), charge transfer resistance (R_{CT}) and Warburg coefficient (Ws1); (D) Calibration curve with increasing molar concentrations of nitrate from 0.6-50 ppm obtained from the CAST-MF sensor. Inset: Binding isotherm representing the correlation between surface coverage (θ) obtained from R_{CT} (Ω) and the respective nitrate concentrations. (E) Amperometry sensing performed at -0.45 V with repeated additions of 0.4 ppm and 1 ppm of nitrate in 0.1 M PBS and pH 6.0 electrolyte.

electrochemical setup, with its sensing electrode unused as observed in Figure 3B. Electrochemical analysis was conducted using 0.5 mL of electrolyte injected through the top slit (sample channel). CV studies showed a decrease in current upon adding a 5 ppm aliquot of nitrate at 50 mV/s (Figure 3B), which was also supported by a continuous increase in R_{CT} upon successive addition of nitrate during EIS (Figure 3C). An inclined line in the lower frequency region of Nyquist plots was maintained at 45°, indicating the penetration of electroactive NO_3^- species into the active Ni@Pani/C nanocomposite.[29]

The calibration curve for nitrate sensing in Figure 3D, shows two different sensitivities with $R_{CT} \approx 2.31 \pm 0.09\ \Omega\ cm^{-2}\ ppm^{-1}$ in the lower concentration range (0.6–10 ppm) and $R_{CT} \approx 0.36 \pm 0.043\ \Omega\ cm^{-2}\ ppm^{-1}$ in the higher concentration range (15–50 ppm), with a low detection limit (LDL) of 0.015 ppm. The varying sensitivities can be attributed to the saturation of active sites on the electrode's surface at higher nitrate concentrations resulting in a slower binding rate. At lower nitrate concentrations, the binding is rapid due to an abundance of active sites and showed a sixfold higher sensitivity. Both linear slopes could be used for sensing nitrate concentration based on ΔR_{CT} in unknown water samples. However, the sensor's dual linear ranges overlap between 10-15 ppm, which may result in lower sensitivity and accuracy in this range and can be addressed by using the statistical model presented as an orthogonal method to analyze the sensor's data within this range. The observed variation in the background R_{CT} values between the two systems presented namely the 75 mL macrosystem in Figure 2D and the 500 µL microsystem in Figure 3D can be due to various reasons such as the difference in electrolyte volume, electrode surface area, type and size of electrodes, proximity of electrodes to name a few. However, since this aspect does not impact the overall nitrate sensing trend which remains consistent, it can be overlooked in this study. In the future studies, we aim to develop a machine learning approach to effectively remove background noise for each system and normalize their responses enabling better comparison. Figure 3D inset shows an adsorption binding isotherm derived from a Langmuir-fitted curve of the EIS sensing response. The mathematical expression for our model is given by the following Langmuir equation[48]:

$$\frac{C}{\theta} = \frac{1}{K_A} + C$$

In this equation, θ is the surface coverage on the Ni@Pani/C sensing electrode based on R_{CT} in the absence and presence of nitrate ($\theta = 1 - R_{CT,0}/R_{CT}$), while C represents the concentration of nitrate and K_A denotes the equilibrium constant of adsorption[48]. The isotherm (Figure 3D inset) displayed a sharp rise in the surface area coverage even at lower nitrate concentrations based on the R_{CT} values from the calibration curve, thereby indicating high affinity and saturation on the sensor surface as nitrate concentration increases. The sensor's

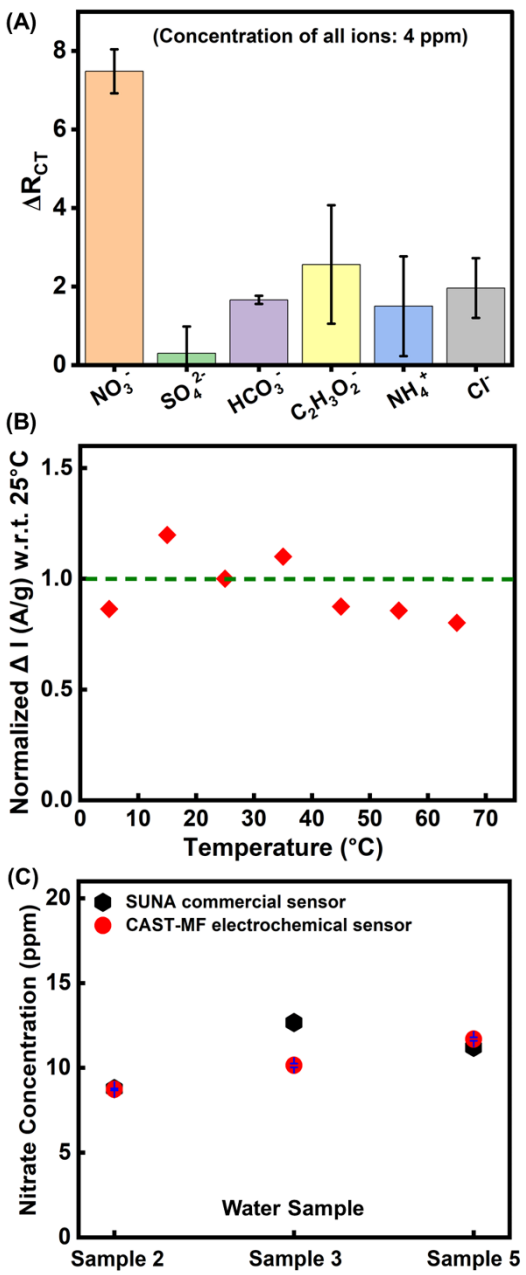

Fig. 4 (A) The CAST-MF sensor's EIS response for 4 ppm nitrate and 4 ppm of interfering ions: sulphate, bicarbonate, acetate, ammonium and chloride; (B) CAST-MF sensor performance at different temperatures maintaining a fixed 2 ppm nitrate concentration; (C) Comparative performance of our CAST-MF electrochemical sensor vs commercial SUNA V2 with stream samples from the Gwynns Falls watershed in Maryland, U.S.A (1 mg N/L = 4.18 ppm).

behavior showed a moderately good fit to the Langmuir curve with a K_A value of 0.0696 and an R^2 value of 0.8057 indicating a possible mix of monolayer and multilayer adsorption at higher nitrate concentrations. Overall, across both ranges together we obtained an RMSE value of 0.0432 indicating high accuracy with small deviation and a reliable model fit. Moreover, a plot of C/θ as a function of C provided an R^2 value of 0.9330 demonstrating a stable and robust nitrate adsorption on the Ni@Pani/C sensing electrode surface[48].

Previously, Pani has been used with MWCNT and Gum Arabic to adsorb and electrocatalytically reduce nitrate as a sensing method.[34] In this study, we focus on enhancing the adsorption dynamics by introducing Ni^{2+} onto the surface of Pani. Ni^{2+} serves as an active site for nitrate ion adsorption through electrostatic interactions following Langmuir-type monolayer adsorption. These Ni^{2+}-NO_3^- surface complexes form an insulating layer that impedes electron transfer at the electrode interface, leading to higher charge transfer resistance (R_{CT}) as nitrate ion availability increases. Consistent with this mechanism, our results show that R_{CT} increases with increase in nitrate concentration, and the sensor response aligns well with the Langmuir adsorption isotherm (Figure 3D inset). This understanding also helps explain the sensor's selectivity towards nitrate ions in the presence of interfering ions. The selectivity primarily depends on the binding interactions with Ni^{2+} and their impact on R_{CT}. While interfering ions may adsorb onto the electrode surface and block nitrate-binding sites leading to reduced sensitivity, they do not replicate the binding dynamics of nitrate or its R_{CT} response.

Figure 3E shows an amperometric study using the CAST-MF sensor with repeated 0.4 ppm and 1 ppm nitrate concentrations. The response time of the CAST-MF sensor upon changing nitrate concentration was observed to be 20 seconds, which is quite rapid for a first-generation prototype and is comparable with the previously reported nitrate and nitrite based electrochemical sensors[13,31,43,49-51]. The response time of the CAST-MF sensor was calculated based on the time required for the sensor to reach 90% of its stable peak current from the point of analyte injection. For example, for the first 0.4 ppm and 1 ppm nitrate injections (Figure 3E) the sensor needed 11.17 seconds and 26.36 seconds respectively to attain 90% of the initial signal. This was followed by 28.88 seconds for the next 1 ppm and 13.24 seconds for the next 0.4 ppm nitrate injections respectively, attributing the decrease in the sensor's response rate to the saturation of binding sites with each consecutive injection. Overall, the average response time of the sensor was calculated to be 20 seconds.

The initial electrochemical sensing tests with the CAST-MF sensor were conducted in N_2-saturated electrolytes to establish a controlled baseline and to understand the sensor's performance without interference from oxygen. This allowed us to isolate and study the sensor's response to nitrate under ideal conditions. However, we recognize that environmental monitoring often occurs in the presence of oxygen, which can indeed influence nitrate measurements.

To address this concern, we conducted additional tests using field water samples without N_2 saturation, and it was observed that the sensor performed reliably in the presence of oxygen, indicating its robustness and applicability for environmental monitoring. While oxygen can influence measurements, our field water tests confirmed that the CAST-MF sensor remained effective in sensing nitrate under typical environmental conditions. We believe this dual approach of controlled lab tests followed by real-world validation provides a comprehensive understanding of the CAST-MF sensor's nitrate sensing capabilities.

Specificity, Stability, Reproducibility and Reusability

The CAST-MF sensor demonstrated good selectivity, stability, reproducibility, and reusability thereby showing potential for commercial usage. Commonly found interfering ions in water such as bicarbonate (HCO_3^-), ammonium (NH_4^+), and chloride (Cl^-) were chosen for this study; along with sulphate (SO_4^{2-}) and acetate ($C_2H_3O_2^-$) that are known to cause interference due to electrostatic interactions and hydrogen bonding with Pani. In the presence of these interfering ions, Ni@Pani/C showed a distinct selectivity towards nitrate ions (Figure 4A). A concentration of 4 ppm (equivalent to ~1 mg N/L) was chosen for this study to evaluate the sensitivity of our sensor towards nitrate detection at a low concentration, despite the presence of other interfering ions at the same concentration. An addition of 4 ppm of each interfering ion caused minimal hindrance to nitrate ion detection (±26% ΔR_{CT}), except in the case of acetate (±34% ΔR_{CT}). However, inhibition of the electrochemical signal upon the interaction of Pani with acetic acid has already been reported[47], and addressing this issue is beyond the scope of our study. The adsorption mechanism presented for sensing with Ni^{2+} is selective for nitrate ions, and we anticipate nitrite will exhibit lower adsorption and charge transfer resistance in comparison. While this manuscript focuses on nitrate sensing, it would be interesting to explore further sensor modifications or machine learning analytics for nitrite detection in the future work. We are further developing a signal processing approach using machine learning to filter out the interfering responses of coexisting substances in field samples based on their specific signal patterns and shapes, thereby enabling us to accurately measure the true response of nitrate. The CAST-MF sensor demonstrated stable nitrate sensing performance over a wide temperature range of 5°-65°C (Figure 4B). This temperature range was chosen based on the reported thermal durability of PMMA which forms the framework of the cassette[52,53].

Reusability of the sensing electrode was studied by recording an EIS response for 26 days (~1 month) with a fixed 1 ppm nitrate concentration (Figure S6A). For this study, the sensor was rinsed with DI water after each study and dried at room temperature before and after each use. Different batches of electrodes exhibited comparable results yielding an average of 1.1-1.5 mg/cm^2 of Ni@Pani/C mass loading in more than 50 electrodes fabricated over multiple batches. These electrodes were stored in ambient air conditions when not in use. The sensor retained an average of 89% of its initial response to nitrate over a prolonged storage time of 26 days, indicating excellent long-term stability and good reproducibility of the sensor's activity. The PMMA cassette also demonstrated significant durability, by remaining recyclable over a period of two months (67 days) (Figure S6B).

Nitrate Monitoring for Field Water Samples

One of the primary objectives of this study was to ensure that the CAST-MF sensor maintained high accuracy in testing water samples prepared in the laboratory and those obtained from surface water streams. We aimed to ensure that the sensor could effectively withstand varying pH conditions, the presence of numerous unknown sediments, and interfering ions in field water samples. To test the practical applicability of the CAST-MF sensor, we conducted tests with water samples collected from local field sites. Samples were collected from streams in the Gwynns Falls watershed near Baltimore, Maryland, U.S.A. (location details provided in Table S1). For comparison, nitrate concentrations of these stream samples were measured using the commercially available SUNA device[54], which reports them as nitrate-nitrogen mg/L (mg N/L). For the ease of comparison, nitrate concentrations obtained from SUNA were converted from 'mg N/L' into 'ppm' (1 mg N/L = 4.18 ppm) in this study. Samples collected were stored by freezing at -4°C in cases where they could not be filtered immediately after collection on the field. They were later thawed and analysed within the first 24-48 hours.

Results obtained from the CAST-MF electrochemical sensor showed good agreement with those obtained from the SUNA V2 device (Figure 4C) with an absolute error of ±2.5 ppm (~0.6 mg N/L) and an average recovery of 91.8%, thereby confirming the accuracy of the CAST-MF sensor for nitrate detection in field samples and its potential for commercialization. Additionally, in comparison to SUNA V2 device, our CAST-MF sensor is more sensitive towards nitrate detection with a low detection limit (LDL) of 0.015 ppm against SUNA V2's LDL of 0.04 ppm (nitrate-nitrogen). Our sensor is a low-cost and portable alternative that has similar potential use as SUNA V2 with future addition of automation and remote data logging that could enable multi-point installation and monitoring the movement of nitrate contamination across the entire stream length. The affordability of our sensor also makes it easily available for agricultural, academic and citizen science applications.

Statistical Model for Prediction of Nitrate Concentration

We utilized the collected data to develop a 3D statistical model that can predict nitrate concentrations in field water samples (Z axis) based on their corresponding R_{CT} values obtained from the CAST-MF sensor. Our objective was to develop a simple and scalable data-driven model that can be used by untrained operators on-site. To further avoid complex post data-acquisition analysis, the Warburg coefficient was eliminated as an independent input variable, since elaborate curve fittings in a spectrum analyzer were needed for its implementation. Instead, R_S (X axis) was chosen as the second independent input variable along with R_{CT} (Y axis), since it accounts for the variable salt concentrations present in field samples that potentially affect ionic activity coefficients and measurement noise, which in turn may affect the measured R_{CT} values. R_S can also be easily obtained from a single impedimetric scan using the CAST-MF sensor. Our exploratory studies of incorporating R_S in the predictive model (Figure 5A) showed that it helped to minimize background noise and bias in model predictions and improved the R^2 value by 6.15% and reduced the RMSE value by 20.59%. Performance of the model or its prediction accuracy can be further enhanced by testing additional field water samples varying in nitrate concentration and background geochemistry.

Sample Number	Sample #ID / Collection Location	Solution Resistance (R_S) (Ω)	Charge Transfer Resistance (R_{CT}) (Ω)	Nitrate Concentration (ppm)		
				CAST-MF Sensor Measurement	Statistical Model Prediction	Absolute Error in Model Prediction
Sample 1	Rutherford	19.67	3.73	0.00	0.61	±0.61
Sample 2	Franklintown	17.15	8.46	2.00	1.89	±0.11
Sample 3	Tributary	16.05	12.96	3.00	3.54	±0.54
Sample 4	Kent Run	19.86	23.02	5.00	4.39	±0.61

Table 1. Test data set to confirm the statistical model's accuracy in predicting nitrate concentrations in comparison to the readings obtained from CAST-MF microfluidic sensor for stream water samples mentioned in Table S1. The samples were diluted and blinded for this study. (Further details can be found in the supporting information.)

Our 3D multiple regression model can generate thousands of Z predictions between two X and Y experimental values and holds potential as a better extrapolation tool compared to a traditional 2D calibration curve. It (i) accounts for non-linearity between input variables, making it applicable for different data sets; (ii) handles two independent variables at a time and accommodates variation in the sensing environment; (iii) reduces bias by eliminating manual adjustments; (iv) provides calibration stability due to minimal sensitivity towards minor outliers, (v) facilitates a simultaneous visualization of the impact of both variables on the model's response, and (vi) provides a direct readout of the predicted value to the user within seconds. Table S1 represents the various field samples collected as described above. Table S2 depicts the training data set prepared from dilutions of these samples to obtain a wide range of nitrate concentrations (ppm). Various second-order non-linear terms were tested using this data to identify the most effective term for enhancing the goodness of the fit (Table S2, Figures S7 and S8). Figure S9 shows the trend of the dependence of predicted nitrate concentration values on R_{CT}.

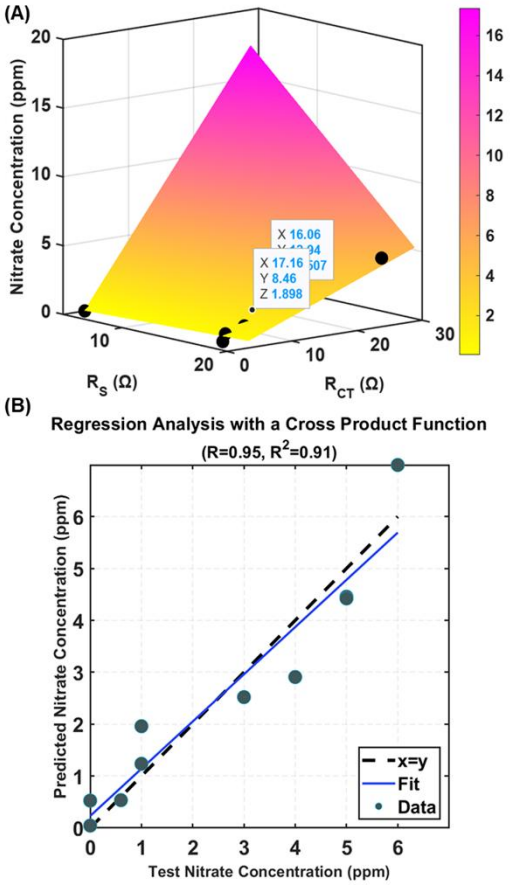

Fig. 5 (A) A 3D mesh plot showing output of the statistical model obtained from multiple regression analysis. R_S (X axis) and R_{CT} (Y axis) represent experimental values obtained from the CAST-MF sensor for stream water samples (Table S2), and Z axis represents their corresponding predicted nitrate concentrations. Extrapolated points for two of the four unknown samples (Table 1) have been highlighted. (B) A 2D regression plot of the predicted nitrate concentrations by the statistical model (Y axis) versus test nitrate concentrations from the CAST-MF sensor (X axis) (Table S2). Regression analysis performed with a non-linear cross-product term (x_1.*x_2) of R_S (x_1) and R_{CT} (x_2) to reduce error in predictions.

To investigate the performance of our model, a two-point cross-validation was performed. Four stream samples were randomly selected from Table S1 and diluted to create blinded concentrations, which were then utilized in the test data set as shown in Table 1. Their respective R_S and R_{CT} output values obtained from the EIS experiments of CAST-MF sensor were substituted in the model's plot to extrapolate predicted nitrate concentrations (Z), highlighted in Figures 5A and S10. The model's predictions were highly comparable with the readings obtained from the CAST-MF sensor and showed an absolute error of ±0.6 ppm as observed in Table 1. Overall, an R^2 value of 0.9101 was obtained (Figure 5B) indicating a high correlation or a good fit of the model's predictions to the actual observed data. This means our model can explain up to 91% of the variation in its predicted nitrate concentrations around their mean value, thereby providing a significant interpretation of the experimental data[55-57].

In this study, we have shown the potential of leveraging the empirical correlations between R_S and R_{CT} as input parameters and the nitrate concentration (ppm) in samples as the response; to develop a simple data-driven multiple regression model that can mathematically confirm the precision in our sensor's readings with reference to experimental results. In future studies, we will explore the potential of machine learning using neural networks or deep learning for recognizing patterns in the sensor's response with respect to changes in pH, sample composition, storage duration, temperature, etc. to increase the reliability in the model's predictions.[56-57] A classifier neural network will be used to sort the predicted nitrate concentrations within a hazard range (good / bad / alarming) and supported with a digital read-out system.

Conclusions

In summary, our study presents a microfluidic electrochemical sensor that provides a cost-effective and environment friendly approach for rapid detection of nitrate using Ni@Pani/C nanocomposite. The microfluidic cassette design, scalable electrode fabrication, and the presence of Pani enabling high selectivity, collectively contribute to the development of a highly sensitive nitrate sensor. A proportional increase in R_{CT} was observed, establishing a clear relationship between the electrochemical signals and increasing nitrate concentration even at sub-ppm levels. Importantly, our sensor showed comparable results with the SUNA V2 commercial device (~91.8% recovery) for determining nitrate concentrations in stream samples from the Baltimore region, Maryland, U.S.A. The sensor could also operate with negligible interference from other ions in the field water samples. It demonstrated remarkable stability over a wide temperature range (5°-65°C) and showed good repeatability in nitrate sensing over several days (~1 month). Having a portable setup, rapid one-step analysis method, and ease of operation by non-trained personnel, the CAST-MF sensor exhibits high potential for commercial application as an on-site nitrate analyzer. With this study, we have also shown that a statistical model using experimentally obtained electrochemical parameters can be used to mathematically confirm the accuracy of our sensor's readings (observed absolute error of ±0.6 ppm). Overall, we have developed a microfluidic (500 µL) sensor that is competent in terms of cost (affordability per sample), dimensions (light, compact and hand-held: 40*4*4 mm, 9.2 g), performance range (low detection limit: 0.015 ppm of nitrate), reliability (reproducible with least possible standard deviation), high precision and a rapid response rate (20 seconds). It has thus demonstrated the potential to be further developed into a flow-cell prototype suitable for automated[58], continuous and real-time monitoring of nitrate[59] at various locations, which is imperative to environmental protection and public health.

Author contributions

S. K. M. writing – original draft, data curation, formal analysis, investigation, methodology, visualization. R. K. writing – original draft, software, conceptualization, data curation, formal analysis, investigation, methodology, visualization. T. P. investigation. P. A. formal analysis, investigation. M. S. resources. J. L. resources. M. T. investigation, resources. M. M. investigation, resources. C.W. writing – review & editing, funding acquisition, resources. D. D. F. writing – review & editing, software, supervision. V. S. writing – review & editing, funding acquisition, supervision, validation, conceptualization, methodology. S. K. U. writing – review & editing, funding acquisition, supervision, validation, visualization, conceptualization, data curation, investigation, methodology, formal analysis. G. R. writing – review & editing, funding acquisition, project administration, conceptualization, supervision.

Conflicts of interest

There are no conflicts to declare.

Data availability

The data supporting this article have been included as part of the Supplementary Information.

Acknowledgements

Authors acknowledge the support from industrial collaborator Dietrich Ruehlmann, Managing Partner at GaiaXus, Maryland. This work has been supported by funding from the Maryland Industrial Partnerships (MIPS) award (#7104), Maryland Innovation Initiative (MII) TEDCO award (0923-0003) and National Science Foundation (NSF) award (#2012340) and DOE award DE-SC0023217.

References

1 K. Obaideen, N. Shehata, E. T. Sayed, M. A. Abdelkareem, M. S. Mahmoud and A. G. Olabi, *Energy Nexus*, 2022, **7**, 100112.
2 Bijay-Singh and E. Craswell, *SN Appl. Sci.*, 2021, **3**, 518.
3 P. Banerjee, P. Garai, N. C. Saha, S. Saha, P. Sharma and A. K. Maiti, *Water, Air, & Soil Pollution*, 2023, **234**, 333.
4 S. S. Bharate, *J. Med. Chem.*, 2021, **64**, 2923–2936.
5 D. A. Hutchins and D. G. Capone, *Nat. Rev. Microbiol.*, 2022, **20**, 401–414.
6 D. Garcia and T. Matthews, *ACS ES&T Water*, 2024, **4**, 3340-3347.
7 R. Felton, B. J. Dalzell, J. Baker, K. D. Flynn and S. A. Porter, *ACS ES&T Water*, 2023, **3**, 3305–3314.
8 H. Xu, Y. Ma, J. Chen, W. Zhang and J. Yang, *Chem. Soc. Rev.*, 2022, **51**, 2710–2758.
9 C. Duan, W. Bai and J. Zheng, *New J. Chem.*, 2018, **42**, 11516–11524.
10 S. F. Johnson, *Curr. Probl. Pediatr. Adolesc. Health Care*, 2019, **49**, 57–67.
11 M. Ward, R. Jones, J. Brender, T. de Kok, P. Weyer, B. Nolan, C. Villanueva and S. van Breda, *Int. J. Environ. Res. Public Health*, 2018, **15**, 1557.
12 E. Abascal, L. Gómez-Coma, I. Ortiz and A. Ortiz, *Sci. Total Environ*., 2022, **810**, 152233.
13 R. K. Amali, H. N, Lim, I. Ibrahim, N. M. Huang, Z. Zainal and S. A. A. Ahmad, *Trends in Environmental Analytical Chemistry*, 2021, **31**, e00135.
14 C. Jiang, Y. He and Y. Liu, *Analyst*, 2020, **145**, 5400-5413.
15 S. A. Glazier, E. R. Campbell and W. H. Campbell, *Anal. Chem.*, 1998, **70**, 1511–1515.
16 K. S. Johnson and L. J. Coletti, *Deep Sea Res. Part I: Oceanogr. Res. Pap.*, 2002, **49**, 1291–1305.
17 M. Badea, A. Amine, G. Palleschi, D. Moscone, G. Volpe and A. Curulli, *J. Electroanal. Chem.*, 2001, **509**, 66–72.
18 A. Charbaji, H. Heidari-Bafroui, C. Anagnostopoulos AND M. Faghri, *Sensors*, 2020, **21**, 102.
19 D. L. Heanes, *Analyst*, 1975, **100**, 316-321.
20 H. Essousi, H. Barhoumi, M. Bibani, N. Ktari, F. Wendler, A. Al-Hamry and O. Kanoun, *J. Sensors*, 2019, **1**, 4257125.
21 S. Butt, *Talanta*, 2001, **55**, 789–797.
22 Y. Michigami, Y. Yamamoto and K. Ueda, *Analyst*, 1989, **114**, 1201-1205.
23 X. Chen, H. Pu, Z. Fu, X. Sui, J. Chang, J. Chen and S. Mao, *Environ. Sci. Nano*, 2018, **5**, 1990–1999.

24 L. Snyder, J. D. Potter and W. H. McDowell, *Water Resour. Res*., 2018, **54**, 2466-2479.
25 A. K. M. S. Inam, M. A. C. Angeli, B. Shkodra, A. Douaki, E. Avancini, L. Magagnin, L. Petti and P. Lugli, *ACS Omega*, 2021, **6**, 33523–33532.
26 Y. Qiu and K. Qu, *Environ. Res.*, 2022, **214**, 114066.
27 D. Micić, B. Šljukić, Z. Zujovic, J. Travas-Sejdic and G. Ćirić-Marjanović, *Electrochim. Acta*, 2014, **120**, 147–158.
28 D. Zhang and Y. Wang, *Mater. Sci. Eng. B*, 2006, **134**, 9–19.
29 S. B. Yoon, E. H. Yoon and K. B. Kim, *J. Power Sources*, 2011, **196**, 10791–10797.
30 R. Djara, Y. Holade, A. Merzouki, N. Masquelez, D. Cot, B. Rebiere, E. Petit, P. Huguet, C. Canaff, S. Morisset, T.W. Napporn, D. Cornu and S. Tingry. *J. Electrochem. Soc.*, 2020, **167**, 066503.
31 H. Wang, P. H. Yang, H. H. Cai and J. Cai, *Synth. Met.*, 2012, **162**, 326–331.
32 H. Bagheri, A. Hajian, M. Rezaei and A. Shirzadmehr, *J. Hazard. Mater.*, 2017, **324**, 762–772.
33 G. Gao, M. Pan and C. D. Vecitis, *J. Mater. Chem. A.*, 2015, **3**, 7575–7582.
34 S. A. M. Kosa, A. N. Khan, S. Ahmed, M. Aslam, W. A. Bawazir, A. Hameed and M. T. Soomro, *Nanomaterials*, 2022, **12**, 3542.
35 W. Chen, R. B. Rakhi, H. N. Alshareef, *J. Phys. Chem. C.*, 2013, **117**, 15009–15019.
36 V. B. Mohan, K. T. Lau, D. Hui and D. Bhattacharyya, *Compos. Part B: Eng.*, 2018, **142**, 200-22.
37 Y. V. M. Reddy, J. H. Shin, V. N. Palakollu, B. Sravani, C. H. Choi, K. Park and N. P. Shetti, *Adv. Colloid Interface Sci.*, 2022, **304**, 102664.
38 M. Ates, A. A. Eker and B. Eker, *J. Adhes. Sci. Technol.*, 2017, **31**, 1977-1997.
39 R. A. Graff, T. M. Swanson and M. S. Strano, *Chem. Mater.*, 2008, **20**, 1824–1829.
40 L. Zhu, Y. Chang, Y. Li, M. Qiao and L. Liu, *Biosensors*, 2023, **13**, 507.
41 W. Yi, Z. Li, W. Dong, C. Han, Y. Guo, M. Liu, C. Dong, *ACS Appl. Nano Mater.*, 2022, **5**, 216–226.
42 J. A. Lori, A. Morrin, A. J. Killard, M. R. Smyth, *Electroanalysis*, 2006, **18**, 77–81.
43 N. S. Al-Kadhi, M. A. Hefnawy, F. S. Alamro, R. A. Pashameah, H. A. Ahmed and S. S. Medany, *Polymers*, 2023, **15**, 1804.
44 S. K. Ujjain, P. Ahuja and R. K. Sharma, *J. Mater. Chem. B.*, 2015, **3**, 7614–7622.
45 L. Brožová, P. Holler, J. Kovářová, J. Stejskal and M. Trchová, *Polymer Degradation and Stability*, 2008, **93**, 592-600.
46 J. A. Bornhorst and J. J. Falke, *Methods in Enzymology*, 2000, **326**, 245-254.
47 L. I. Briel, *U.S. Geological Survey*, 1997, **1422**, doi.org/10.3133/pp1422D.
48 A. Toghan, M. Khairy, M. Huang, and A. A. Farag, *International Journal of Electrochemical Science,* **2023**, *18*(3), 100072.
49 M. Muchindu, T. Waryo, O. Arotiba, E. Kazimierska, A. Morrin, A. J. Killard and E. I. Iwuoha, *Electrochim. Acta*, 2010, **55**, 4274-4280.
50 M. Guo, J. Chen, J. Li, B. Tao and S. Yao, *Anal. Chim. Acta*, 2005, **532**, 71-7.
51 X. Luo, A. J. Killard and M. R. Smyth, *Chem. Eur. J.* 2007, **13**, 2138-2143.
52 A. Andar, M. S. Hasan, V. Srinivasan, M. Al-Adhami, E. Gutierrez, D. Burgenson, X. Ge, L. Tolosa, Y. Kostov, G. Rao, Wood Microfluidics. *Anal. Chem.*, 2019, **91**, 11004–11012.
53 M. S. Hasan, S. B. Borhani, S. S. Ramamurthy, A. Andar, X. Ge, F. S. Choa, Y. Kostov and G. Rao, *Sci. Rep.*, 2022, **12**, 16075.
54 C. Welty, J. Moore, D. J. Bain, M. Talebpour, J. T. Kemper, P. M. Groffman and J. M. Duncan, *Water Resour. Res.*, 2023, **59**, e2021WR031804.
55 K. A. Vakilian and J. A. Massah, *IEEE Sens. J.*, 2018, **18**, 3080-3089.
56 K. A. Vakilian, J. A. Massah, *IEEE Sens. J.*, 2018, **18**, 3080-3089.
57 J. Massah and K. A. Vakilian, *Biosyst. Eng.*, 2019, **177**, 49-58.
58 H. Hasan, V. Kumar, X. Ge, C. Sundberg, C. Slaughter, G. Rao, *Biosens. Bioelectron.*, 2024, **253**, 116138.
59 K. Lal, S. A. Jaywant and K. M. Arif, *Sensors*, 2023, **23**, 7099.

The data supporting this article have been included as part of the Supplementary Information.